J|A|C|S
ARTICLES

Published on Web 06/24/2010

Morphology Control of Nanostructures via Surface Reaction of Metal Nanodroplets

K.Y. Niu,[†] J. Yang,[†] S. A. Kulinich,[‡,§] J. Sun,[†] H. Li,[†] and X. W. Du*[,†]

School of Materials Science and Engineering, Tianjin University, Tianjin 300072, People's Republic of China, Department of Chemistry, University of British Columbia, Vancouver, BC, Canada V6T 1Z1, and Department of Applied Sciences, University of Quebec, Saguenay, PQ, Canada G7H 2B1

Received April 8, 2010; E-mail: xwdu@tju.edu.cn

Abstract: We report on the controllable synthesis of diverse nanostructures using laser ablation of a metal target in a liquid medium. The nanodroplets generated by laser ablation react with the liquid and produce various nanostructures, such as hollow nanoparticles, core−shell nanoparticles, heterostructures, nanocubes, and ordered arrays. A millisecond laser with low power density is essential for obtaining such metal nanodroplets, while the target material, the reactivity of liquid medium, and the laser frequency are decisive for controlling the morphology and size of the nanostructures produced. This green and powerful technique can be extended to different material systems for obtaining various nanostructures.

Introduction

The morphology of nanostructured materials has a remarkable influence on their properties. Hence, the controllable synthesis of nanostructures has become a consistent ambition in the nanoworld.[1,2] Currently, the control of nanostructures is usually achieved via tunable chemical reactions.[2,3] A more facile and greener method, pulsed laser ablation in liquid (PLAL), has been recently developed to synthesize nanoparticles, in which a pulsed laser is adopted to irradiate a solid target in a liquid medium.[4−7] Plasma and vapor, as well as metal droplets, were reported as possible ablation products, which further react with the liquid medium to form nanoparticles.[5,6,8−10] Among these three, plasma was considered as an ideal starting phase for the synthesis of nanomaterials, because it can vaporize the surrounding liquid medium[6,11] and then mix and react with the vapor in a penetrating way (hereafter, this reaction is referred to as *penetration reaction*). Therefore, much attention has been paid to generating the plasma by using short-pulse-width lasers, for example, a nanosecond pulsed laser with pulse width of several nanoseconds and power density of 10^8-10^{10} W/cm^2. This could provide high energy flux in a short time window to generate plasma, and indeed, ultrafine colloidal metal and compound nanoparticles were fabricated.[6,12−15] During the past two decades, the products of PLAL were mainly limited to the above two categories, and new products were seldom reported.[16] So far, morphology control of nanostructures has never been realized by the PLAL method, and it was doubtful whether this technique had the capability of producing novel nanostructures.

If we turn our attention to the metal droplets potentially produced during PLAL treatment of a metal target, the situation could be remarkably different. The temperature of such metal droplets is much lower than that of the plasma. As a result, any reactions with the ambient medium are expected to start from the surface of such droplets due to their compactness (hereafter, such reactions are referred to as *surface reactions*). Therefore, the mode and extent of surface reactions can be controlled by precisely selecting appropriate types and concentrations of the liquid media, as well as the laser parameters. Then the question is simply how to generate pure metal droplets and design droplet−liquid reaction systems giving rise to nanostructures sought.

In the present work, we utilize a laser with a long pulse width, that is, a millisecond pulsed laser, to generate metal nanodroplets in liquids. Such a laser is commonly used for welding but seldom for the synthesis of nanomaterials. Due to its lower

[†] Tianjin University.
[‡] University of British Columbia.
[§] University of Quebec.

(1) Arico, A. S.; Bruce, P.; Scrosati, B.; Tarascon, J. M.; Van Schalkwijk, W. *Nat. Mater.* **2005**, *4*, 366–377.
(2) Lou, X. W.; Archer, L. A.; Yang, Z. C. *Adv. Mater.* **2008**, *20*, 3987–4019.
(3) Peng, X. G.; Manna, L.; Yang, W. D.; Wickham, J.; Scher, E.; Kadavanich, A.; Alivisatos, A. P. *Nature* **2000**, *404*, 59–61.
(4) Patil, P. P.; Phase, D. M.; Kulkarni, S. A.; Ghaisas, S. V.; Kulkarni, S. K.; Kanetkar, S. M.; Ogale, S. B.; Bhide, V. G. *Phys. Rev. Lett.* **1987**, *58*, 238–241.
(5) Kazakevich, P. V.; Simakin, A. V.; Voronov, V. V.; Shafeev, G. A. *Appl. Surf. Sci.* **2006**, *252*, 4373–4380.
(6) Yang, G. W. *Prog. Mater. Sci.* **2007**, *52*, 648–698.
(7) Qin, W. J.; Kulinich, S. A.; Yang, X. B.; Sun, J.; Du, X. W. *J. Appl. Phys.* **2009**, *106*, 114318.
(8) Nichols, W. T.; Sasaki, T.; Koshizaki, N. *J. Appl. Phys.* **2006**, *100*, 114911.
(9) Nichols, W. T.; Sasaki, T.; Koshizaki, N. *J. Appl. Phys.* **2006**, *100*, 114912.
(10) Nichols, W. T.; Sasaki, T.; Koshizaki, N. *J. Appl. Phys.* **2006**, *100*, 114913.
(11) Sakka, T.; Iwanaga, S.; Ogata, Y. H.; Matsunawa, A.; Takemoto, T. *J. Chem. Phys.* **2000**, *112*, 8645–8653.
(12) Thareja, R. K.; Shukla, S. *Appl. Surf. Sci.* **2007**, *253*, 8889–8895.
(13) Tsuji, T.; Okazaki, Y.; Tsuboi, Y.; Tsuji, M. *Jpn. J. Appl. Phys.* **2007**, *46*, 1533–1535.
(14) Kabashin, A. V.; Meunier, M. *J. Appl. Phys.* **2003**, *94*, 7941–7943.
(15) Liu, P. S.; Cai, W. P.; Zeng, H. B. *J. Phys. Chem. C* **2008**, *112*, 3261–3266.
(16) Liu, P.; Cao, Y. L.; Wang, C. X.; Chen, X. Y.; Yang, G. W. *Nano Lett.* **2008**, *8*, 2570–2575.

 10.1021/ja102967a

Table 1. Products of Laser Ablation of Pb Target[a]

target	liquid media	laser frenquency (Hz)	results
Pb	dodecyl mercaptan/ *n*-hexane (1:5 v/v)	1	Pb/PbS CSNPs
	mercaptoacetic acid	1	PbS HNPs
	dodecyl mercaptan	1	PbS nanocubes
	mercaptoethanol	20	Pb-PbS heterostructures
	dodecyl mercaptan/ *n*-hexane (1:5 v/v)	20	PbS polycrystalline nanotubes
	dodecyl mercaptan	20	arrays of nanocrystals

[a] Note: PbS HNPs could aslo be produced in dodecyl mercaptan/ *n*-hexane (3:1 v/v) but with poor purity.

Table 2. Products Prepared by Ablating Other Metal Targets

targets	liquid media	laser frenquency (Hz)	results
Mg	ethanol/*n*-hexane (1:5 v/v)	1	MgO HNPs
	ethanol	1	MgO nanocubes
Zn	ethanol/water (10:1 v/v)	1	Zn/ZnO CSNPs
	mercaptoethanol	1	ZnS HNPs
	ethanol/water (10:1 v/v) with addition of ferrocene (2 mmol/mL)	20	ZnO HNPs
	dodecyl mercaptan	1	ZnS nanocrystals
Ni	water	20	NiO nanocubes
Cu	1-dodecanethiol	20	CuS polycrystalline nanowires
Fe	ethanol/water (5:1 v/v)	1	Fe/Fe_xO_y CSNPs

power density (i.e., 10^6-10^7 W/cm^2), metal nanodroplets (rather than vapor or plasma) are expected to be generated, and they are shown to further transform into various nanostructures through surface reactions with liquid media. The obtained nanostructures include core−shell nanoparticles (CSNPs), nanocubes, tube-like nanostructures and nanowires, heterostuctures, hollow nanoparticles (HNPs), and ordered arrays of nanoparticles. Our experimental results indicate that surface reactions arising from laser ablation are an effective way toward diverse highly anticipated nanostructures.

Experimental Section

Experiment. Pb, Zn, Mg, Fe, Cu, and Ni targets (purity quotient 99.99%) were ablated by a millisecond pulsed Nd:YAG laser (1064 nm) in liquids with a depth of a 5 mm. The compositions of liquid media used for each target are listed in Tables 1 and 2. The laser power density, work current, pulse width, and irradiation time for all PLAL experiments were set as 10^6 W/cm^2, 200 A, 1 ms, and 5 min, respectively. The target was kept static (and liquid was not agitated) during the laser ablation experiments. For the laser ablation of Ti target in the double-layer liquid medium, the thickness of both hexane and water layers was 3 mm, and the products were collected from each layer using a syringe. The laser pulse width and laser power density in the experiment with a nanosecond laser were selected as 10 ns and 10^8 W/cm^2, respectively.

Measurements and Analysis. The product morphology was determined by using an FEI Technai G2 F20 TEM equipped with a field emission gun, and its composition was analyzed with an Oxford INCA energy-dispersive X-ray spectroscopy module attached to the TEM. The phase structure was investigated by using a Rigaku D/max 2500v/pc X-ray diffractometer. The fast photography was carried out by using a high speed video camera (PHOTRON FAST CAM-SUPER 10KC, Japan). Magnetic properties were detected in a Physical Property Measurement System (PPMS-9T, Quantum Design Co.). The product yield, upon centrifugation, washing in ethanol, and drying, was found to be on the order of tens of milligrams per hour, varying for different structures and material systems.

Results and Discussion

To demonstrate the capability of the proposed technique, we first produce a variety of PbS nanostructures by ablating a Pb target in different liquid media (see Table 1). First, we set the laser frequency as 1 Hz and selected three sulfur-containing liquids with gradually increasing reactivity, that is, dodecyl mercaptan/*n*-hexane (1:5 v/v), mercaptoacetic acid, and dodecyl mercaptan, producing Pb−PbS CSNPs, PbS HNPs, and PbS nanocubes, respectively (Figures 1a−f). We then increased the laser frequency to 20 Hz and ablated the Pb target in the same three liquid media. As a result, Pb−PbS heterostructures are generated in mercaptoethanol (Figure 1g); in the dodecyl mercaptan/*n*-hexane mixture, PbS tube-like nanostructures composed of nanocrystals are obtained (Figure 1h), while in dodecyl mercaptan, a large amount of PbS nanocrystals with uniform size assemble into ordered arrays (Figure 1i).

In other material systems, the PLAL technique showed similar capability of producing different nanostructures (see Table 2). For a Mg target in liquid media with different oxidizing potential, that is, in *n*-hexane/ethanol solution (5:1 v/v) and pure ethanol, MgO HNPs and MgO nanocubes were produced, respectively (Figure 2 and Supporting Information, Figure S1). For a Zn target, we changed the reaction modes by adopting the ambient media of ethanol/water solution (10:1 v/v) and mercaptoethanol, which led to Zn/ZnO CSNPs and ZnS HNPs, respectively (Figure 3 and Supporting Information, Figure S2).

As for the formation mechanism of the above nanostructures, three pieces of evidence support that they originate from metal nanodroplets rather than from vapor or plasma. First, high-speed photography was applied to record real-time images of laser ablation (see such photographs for Ti target are in Figure 4a). During a laser pulse with the width of 2 ms, the target was first heated to its melting point quickly, after which a metal droplet with a size of about 0.6 mm was seen to be ejected within 0.2 ms and stay visible until the end of the laser pulse. At the same time, many smaller microsized droplets were found in the vicinity of the large one, as seen in Figure 4a, 0.2 to 2.0 ms. No plasma plume with a bubble shape (usually observed under nanosecond pulsed laser ablation conditions) is seen in Figure 4a.[17,18] This finding suggests that the nanostructures originate not from the plasma but rather from the metal droplets, although such nanodroplets cannot be observed in the real-time images due to their small size (only microdroplets are seen in Figure 4a).

Second, the formation of CSNPs and HNPs provides direct evidence for the surface reactions between the liquid medium and metal nanodroplets. If the ablation products were vapor or plasma, the penetration reactions would be expected and result in the formation of compound nanoparticles.[7,19] However, if metal nanodroplets are produced by laser ablation, the surface reactions are expected, where the metal droplets are partially oxidized on their surface and give rise to CSNPs. In the systems Pb/S, Mg/O, and Zn/S, where the Kirkendall effect is expected to take place,[20−22] CSNPs can transform into HNPs due to the

(17) Saito, K.; Takatani, K.; Sakka, T.; Ogata, Y. H. *Appl. Surf. Sci.* **2002**, *197*, 56–60.
(18) Tsuji, T.; Tsuboi, Y.; Kitamura, N.; Tsuji, M. *Appl. Surf. Sci.* **2004**, *229*, 365–371.
(19) Barcikowski, S.; Devesa, F.; Moldenhauer, K. *J. Nanopart. Res.* **2009**, *11*, 1883–1893.
(20) Wang, Y. L.; Cai, L.; Xia, Y. N. *Adv. Mater.* **2005**, *17*, 473–477.

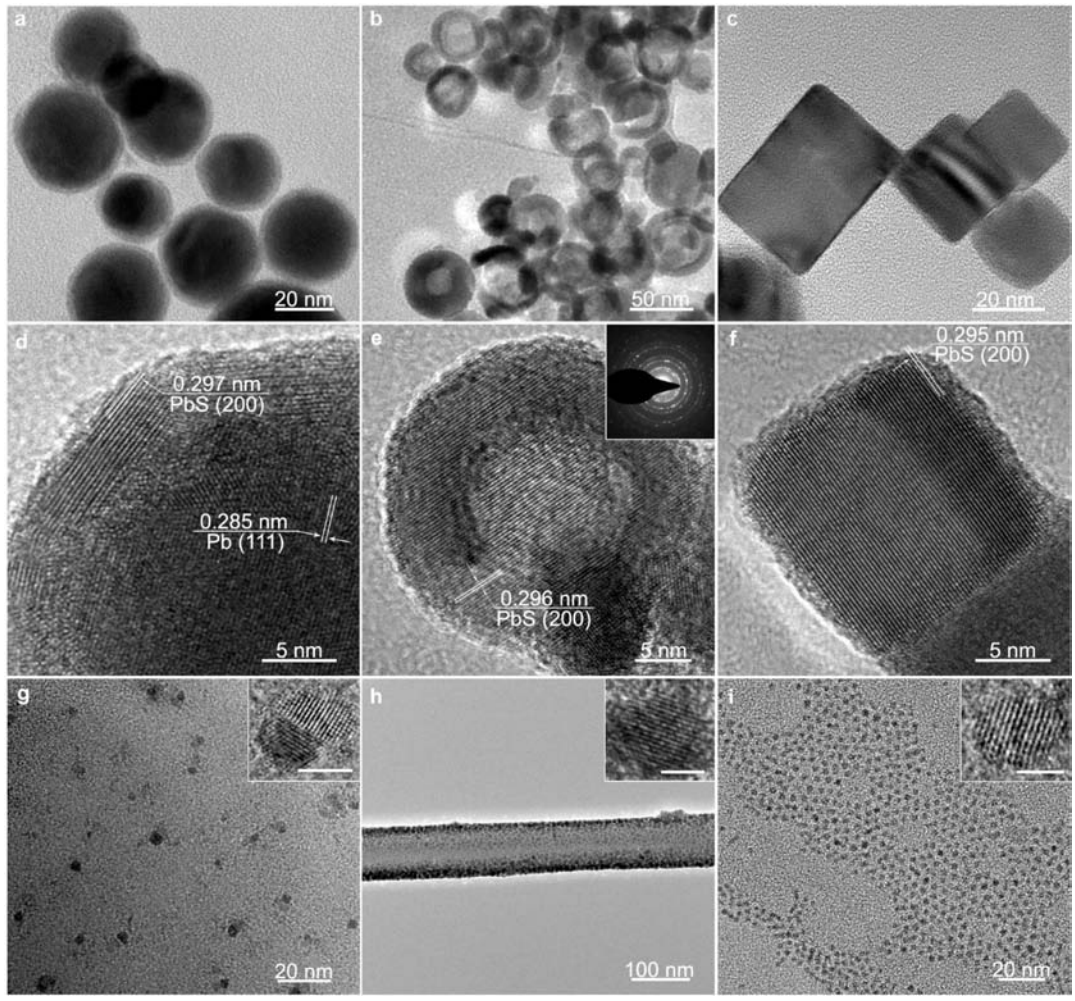

Figure 1. TEM images of various nanostructures obtained in Pb/S system: (a) CSNPs with Pb core and PbS shell; (b) PbS HNPs; (c) PbS nanocubes; (d, e, f) high-resolution TEM (HRTEM) images of the nanostructures in panels a, b, and c, respectively; (g) Pb−PbS heteronanostructures (inset is a HRTEM image of a Pb−PbS nanoparticle; the scale bar indicates 3 nm); (h) a PbS polycrystalline nanotube (inset is a HRTEM image of a nanoparticle in the nanotube; scale bar indicates 3 nm); (i) ordered arrays of PbS nanocrystals (inset is a HRTEM image of such a nanocrystal; scale bar indicates 3 nm).

faster outward diffusion of metal cores and the slower inward diffusion of O or S atoms.[23,24] Amazingly, both the CSNPs formation and their transformation to HNPs may happen within the very same laser pulse, provided that CSNPs with proper shell thickness are first generated. The latter necessity of "appropriate" CSNPs dictates the careful selection of the liquid medium, as both under- and overoxidized nanoparticles cannot be turned into hollow structures (see Figures 1a,c).

Third, we designed an experiment with laser ablation in a double-layer liquid to demonstrate the explosive ejection of the metal nanodroplets. A titanium target was put into a mixture of *n*-hexane and water. Due to the immiscibility and density difference of the two liquids, the mixture separated into a bottom water layer and a top hexane layer, with both layers having the thickness of 3 mm. In such a double-layer medium, if plasma is generated, it must be confined in the water layer and be oxidized into pure TiO_2 nanoparticles via the penetration reaction. Meanwhile, metal nanodroplets generated in such a system would be explosively ejected into both (water and

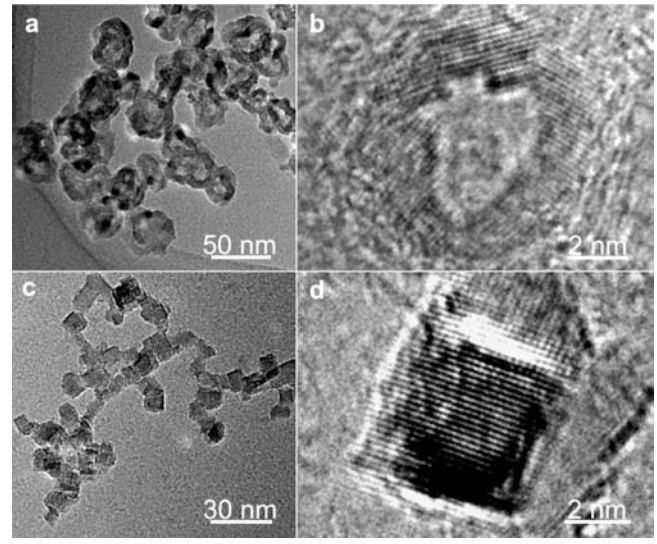

Figure 2. TEM images of MgO nanostructures: (a) MgO HNPs; (b) HRTEM image of a MgO hollow nanoparticle; (c) MgO nanocubes; (d) HRTEM image of a MgO nanocube.

(21) Kooi, B. J.; Palasantzas, G.; De Hosson, J. T. M. *Appl. Phys. Lett.* **2006**, *89*, 161914.
(22) Shao, H. F.; Qian, X. F.; Zhu, Z. K. *J. Solid. State Chem.* **2005**, *178*, 3522–3528.
(23) Fan, H. J.; Gosele, U.; Zacharias, M. *Small* **2007**, *3*, 1660–1671.
(24) Fan, H. J.; Knez, M.; Scholz, R.; Hesse, D.; Nielsch, K.; Zacharias, M.; Gosele, U. *Nano Lett.* **2007**, *7*, 993–997.

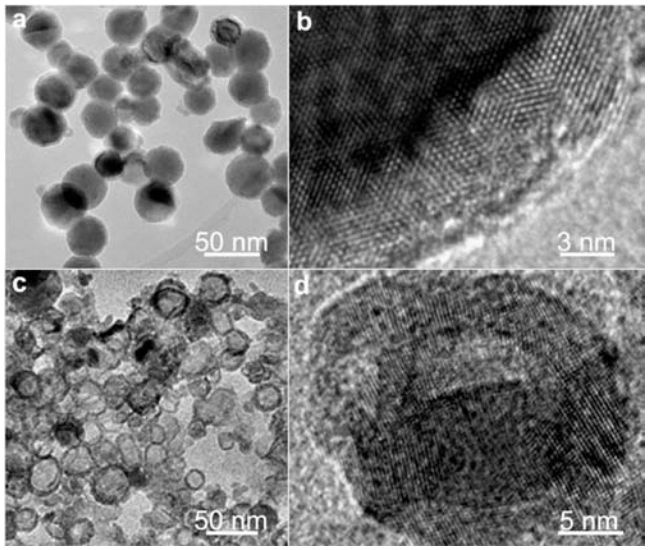

Figure 3. TEM images of Zn nanostructures: (a) Zn/ZnO CSNPs prepared in ethanol/water (10:1 v/v); (b) HRTEM image of the edge of a CSNP; (c) ZnS HNPs prepared in mercaptoethanol; (d) HRTEM image of a half Zn/ZnS CSNP found in the sample of ZnS HNPs.

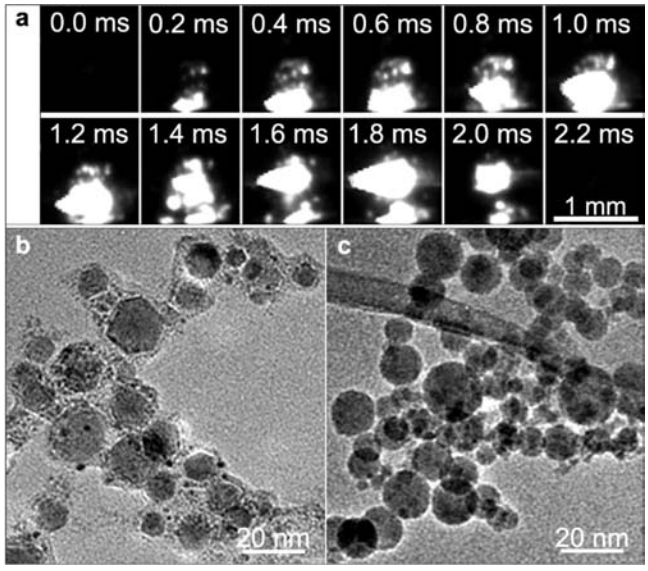

Figure 4. Metal droplets of Ti ablated in a two-layer liquid and their products: (a) time-resolved images of laser ablation of a Ti target in water; (b) TEM image of the carbon-encapsulated Ti nanoparticles formed in the hexane layer of the double-layer liquid medium; (c) TEM image of TiO_2 nanospheres formed in the water layer of the same double-layer liquid medium.

hexane) layers, in agreement with Figure 4a. The surface reactions of such nanodroplets with water and hexane should result in TiO_2 nanoparticles and carbon-encapsulated Ti nanoparticles, respectively. We analyzed products found in both layers, and observed carbon-encapsulated Ti nanoparticles in the hexane layer (Figure 4b and Supporting Information, Figure S3a) and TiO_2 nanospheres in the water layer (Figure 4c and Supporting Information, Figure S3b). Interestingly, when some high-temperature Ti nanodrolpets were ejected into the hexane layer, the decomposed organic molecules assembled as carbon nanotubes (see Supporting Information, Figure S3c,d), thus marking trajectories of the nanodroplets moving through the hexane layer. The above results strongly support our hypothesis

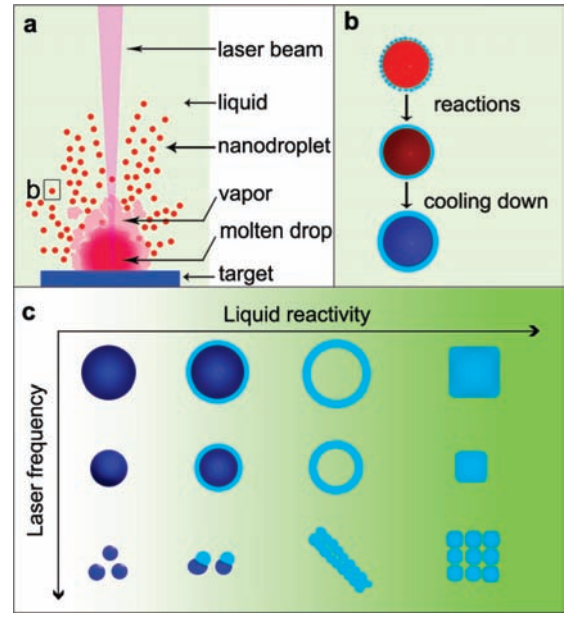

Figure 5. Schematic diagrams of metal nanodroplet ejection and nanostructure formation: (a) formation of nanodorplets in the millisecond-laser-ablation process; (b) reactions of ejected metal nanodroplet with ambient liquid; (c) effect of liquid reactivity and laser frequency on morphology of nanostructures formed in Pb/S system.

on the explosive ejection of metal nanodroplets generated by millisecond laser ablation of metals in liquid.

On the basis of the above results, we propose the following mechanism of formation of the nanostructures observed. When the laser irradiates a metal target in a liquid medium, the local area around the laser spot melts, and a primary metal droplet (with millimetric size, Figures 4a and 5a) first forms. It boils the surrounding liquid medium and produces high-pressure vapor due to the confinement of the liquid layer. The high-pressure vapor causes a strong shattering effect, which results in explosive ejection of a large number of metal nanodroplets from the primary millimetric droplet (Figure 5a). Subsequently, surface reactions between the metal nanodroplets and the ambient liquid take place (Figure 5b). Both composition and morphology of the products are governed by laser parameters applied as well as the nature of target and liquid medium, giving rise to various nanostructures observed (Figures 1 and 5c).

Figure 5c presents schematically the diverse nanostructures prepared in the Pb/S system as a function of liquid reactivity and laser pulse frequency. The reactivity of liquid media is seen to be decisive for the final structure of the products. As the reactivity of the liquid media increases, the surface reactions are seen to advance faster and deeper. As a result, the as-produced nanostructures vary first from pure Pb nanoparticles to Pb/PbS CSNPs. Further increase in the reactivity leads to the rapid formation of a compact PbS shell on Pb core at high temperatures, which allows the Kirkendall voiding and the appearance of PbS HNPs during the same laser pulse. Finally, when the most reactive liquid was used, the Pb nanodroplets were completely sulfidized into perfect single-crystal PbS nanocubes at high temperatures.

On the other hand, the laser frequency also shows a significant effect on the size and morphology of the products. When the laser frequency is low, the as-formed products can move away from the irradiated area before the arrival of the next pulse, thus the initial as-produced nanostructure can be maintained with

higher probability. In contrast, the as-produced nanostructures are more likely to suffer from the secondary irradiation by the next pulse when higher laser frequencies are applied. Therefore, some of them (pure Pb nanoparticles, pure PbS nanocubes) were destroyed into smaller nanoparticles with the same structure as the primary ones, while some others (Pb/PbS CSNPs, PbS HNPs) were destroyed and transformed into new fine nanostructures (Pb−PbS heterostructures, hybrid nanotubes). The formation of such PbS tube-like nanostructures is not well understood yet. It is believed that they could arise from a template effect of the organic mixture used as liquid medium, similar to the colloidal templates formed by surfactant molecules.[25] More specifically, polar dodecyl mercaptan molecules could orient in nonpolar *n*-hexane and form columnar configurations. Very small PbS nanoparticles (inset in Figure 1h) could disperse in such columns of dodecyl mercaptan and follow their geometry, being bonded to their mercapto groups. This was not observed at the low laser frequency since the particles formed were significantly bigger and less mobile to form such tube-like nanostructures.

The above interpretation can be safely expanded to other material systems, for example, Mg/O and Zn/S, and can explain the formation of MgO HNPs, ZnS HNPs, Zn/ZnO CSNPs, and MgO nanocubes. Moreover, based on the above-described mechanism, many other nanostructures were predicted, designed and then prepared in other material systems, such as CuS polycrystalline nanowires, Fe/Fe_xO_y core/shell nanospheres, NiO nanocubes (Supporting Information, Figure S4, and Table 2).

To reveal the advantage of the long-pulse-width (millisecond) laser on controllable synthesis of nanostructures, a short-pulse-width laser, that is, a nanosecond pulsed laser with pulse width of 10 ns and power density of 10^8 W/cm^2, was also used to ablate Mg and Zn targets. The products exhibited obvious inhomogeneity compared with those produced by the long-pulse-width laser (Figure 6). In the Mg/O system, MgO nanoparticles were mixed with MgO HNPs (Figures 6a−c), while in the Zn/O system, a mixture of ZnO nanoparticles with Zn−ZnO CSNPs (Figures 6d−f) was obtained. The HNPs and CSNPs observed are believed to arise from the surface reactions of the nanodroplets, while the MgO and ZnO nanoparticles can be ascribed to the penetration reaction of the plasma. Hence, the short-pulse-width laser with higher power density, while ablating the metal target, generates both plasma and nanodroplets, which leads to less control over the product.

The above results suggest that the proposed synthetic technique based on the use of the millisecond laser provides a number of advantages for the preparation of various nanostructures. First, because of its lower power density, the surface reactions can be realized by using this kind of laser irradiation without any influence of the penetration reaction, which guarantees the product homogeneity. Second, the surface reactions can be easily controlled to obtain different nanostructures by simply changing liquid media or laser parameters. Third, due to the longer pulse width, the efficiency of the long-pulse-width laser ablation is conceivably higher than that of the short-pulse-width laser ablation. Therefore, the long-pulse-width laser is shown to be a better alternative for morphology control of the different nanostructures produced by the PLAL method.

The significance of structure control described in this study is demonstrated in Figure 7, where magnetic properties of different nanostructures (with same composition) are compared.

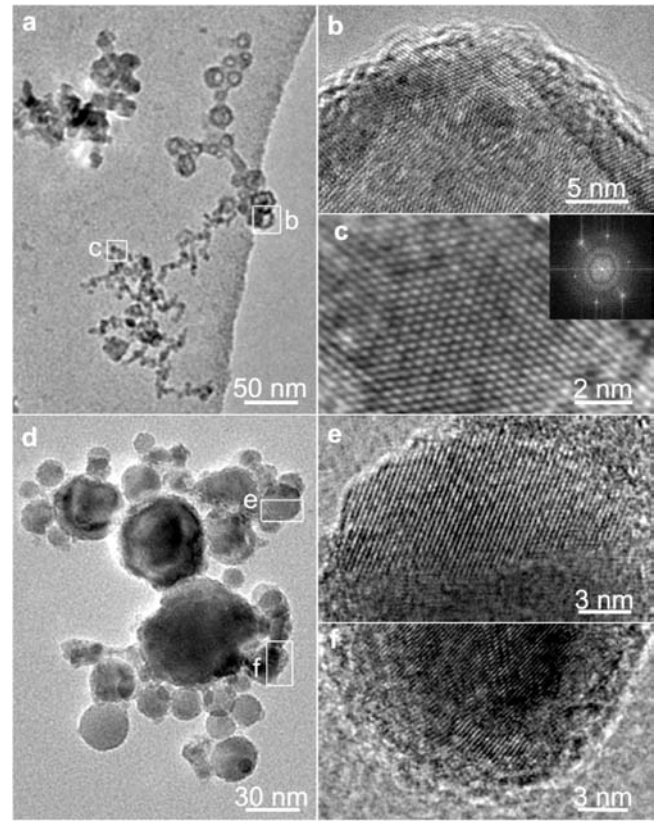

Figure 6. TEM images of products of Mg and Zn target ablation by a nanosecond laser: (a) MgO HNPs and MgO nanoparticles ablated from Mg target; (b) HRTEM image of a MgO HNP; (c) HRTEM image of a MgO nanoparticle along the [0$\bar{2}$2] axis (inset is the corresponding fast-Fourier-transform pattern); (d) ZnO nanoparticles and Zn−ZnO CSNPs ablated from Zn target; (e) HRTEM image of a ZnO nanoparticle; (f) HRTEM image of a Zn−ZnO CSNP.

Different nanostructures with the same composition exhibit significantly disparate ferromagnetic features. For the MgO materials measured at 305 K, the saturation magnetic moment of the HNPs is $\sim 2.5 \times 10^{-4}$ emu/g, which is about 30 times larger than that of the nanocubes ($\sim 0.75 \times 10^{-5}$ emu/g) (Figure 7a,b). For the ZnO materials measured at 5 K, the saturation magnetic moment of the HNPs is ~1.5 emu/g, 7.5 times larger than that of the Zn−ZnO core/shell nanostructures (~0.2 emu/g) (Figure 7c,d). For the ZnS materials measured at 5 K, the hysteresis of the ZnS HNPs is obviously larger and clearer than that of the ZnS nanocrystals, and the corresponding coercivity of the ZnS HNPs (~250 Oe) is about 2.5 times larger than that of the ZnS nanocrystals (100 Oe) (Figures 7e,f). For these inorganic nanomaterials, which are intrinsically nonmagnetic, the ferromagnetism can be ascribed to their surface defects of different type and density,[26−30] which are induced during the surface reactions and subsequent quenching. The fast cooling of the nanostructure surface could induce many defects in the surface atomic layers (see Figure S5c in Supporting Informa-

(25) Pileni, M. P. *Nat. Mater.* **2003**, *2*, 145–150.
(26) Nikolov, A. S.; Atanasov, P. A.; Milev, D. R.; Stoyanchov, T. R.; Deleva, A. D.; Peshev, Z. Y. *Appl. Surf. Sci.* **2009**, *255*, 5351–5354.
(27) Sundaresan, A.; Rao, C. N. R. *Solid. State Commun.* **2009**, *149*, 1197–1200.
(28) Sundaresan, A.; Bhargavi, R.; Rangarajan, N.; Siddesh, U.; Rao, C. N. R. *Phys. Rev. B* **2006**, *74*, 161306.
(29) Jin, H.; Dai, Y.; Huang, B. B.; Whangbo, M. H. *Appl. Phys. Lett.* **2009**, *94*, 162505.
(30) Sundaresan, A.; Rao, C. N. R. *Nano Today* **2009**, *4*, 96–106.

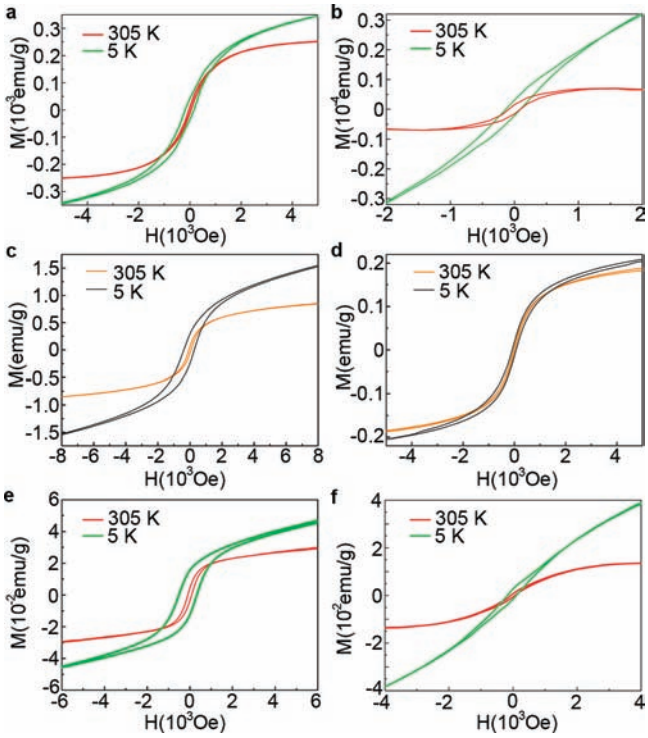

Figure 7. Magnetic properties of as-produced nanostructures: (a) MgO HNPs; (b) MgO nanocubes; (c) ZnO HNPs; (d) Zn−ZnO core/shell nanospheres; (e) ZnS HNPs; (f) ZnS nanocrystals.

tion). It resulted, sometimes, even in amorphous shells on surfaces, such as PbO shells on Pb cores (Supporting Information, Figure S5a,b). Accordingly, ferromagnetism could be induced as a result of numerous defects on the product surface, which is well consistent with the previous report by others.[28] Further research on the magnetic properties is still needed in order to understand the ferromagnetism in such nanostructures in more detail. Other properties, which are also structure dependent, are still to be investigated, while the technique described in this study is shown to provide an excellent opportunity to produce various nanostructrues with similar chemistry. Because of the extreme simplicity, versatility, and efficiency of the technique, such nanostructures can be of wide interest for both fundamental research and practical applications.

Conclusions

In summary, controllable synthesis of nanostructures was accomplished by adopting a long-pulse-width laser to ablate metal target in liquids. Diverse nanostructures, including hollow nanoshperes, core/shell nanospheres, heterostructures, nanocubes, nanowires, and three-dimensional arrays, were produced by carefully selecting metal targets, liquid media, and laser frequency. The nanostructures were demonstrated to be produced via surface reactions of metal nanodroplets ejected from the molten target. Specifically, the final structure of the products is determined by the mode and extent of such surface reactions. A lower power density of the pulsed laser is crucial for generating metal nanodroplets (while excluding plasma or vapor) and thus is decisive for the controllable synthesis of homogeneous nanostructures. Because of its simplicity, versatility, and efficiency, this technique is believed to be a very promising way to synthesize various nanostructures in different material systems. In combination with the minimum chemicals involved, this approach can open a new avenue for the green synthesis of nanomaterials.[19]

Acknowledgment. This work was financially supported by the Natural Science Foundation of China (Nos. 10732020 and 50972102) and National High-Tech R&D Program of China (Nos. 2007AA021808 and 2009AA03Z301).

Supporting Information Available: Experimental details and structure characterizations of the as-produced nanostructures. This material is available free of charge via the Internet at http://pubs.acs.org.

JA102967A